Submitted to

International Europhysics Conference on High Energy Physics, July 12, 2001, Budapest
EPS 2001: Abstract: **801**
Parallel Session **1,2**

XX International Symposium on Lepton and Photon Interactions, July 23, 2001, Rome
LP 2001: Abstract: **493**
Plenary Session **S08**

www-h1.desy.de/h1/www/publications/conf/conf_list.html

Measurement of the Proton Structure Function Using Radiative Events at HERA

H1 Collaboration

Abstract

Deep-inelastic electron-proton scattering (DIS) with initial state photon radiation is investigated using the H1 detector at HERA. The proton structure function $F_2(x, Q^2)$ is measured for Bjorken-x values of $2 \cdot 10^{-5} \leq x \leq 2 \cdot 10^{-2}$ over a Q^2 range extending from 20 GeV^2, where perturbative QCD calculations are clearly valid, down to 0.35 GeV^2, where the influence of non-perturbative effects is large and only phenomenological models can describe the data.

1 Introduction

The study of deep-inelastic lepton-proton scattering (DIS) provides important information that is crucial to our understanding of proton structure. Since the first observation by the HERA ep experiments [1, 2] of the strong rise of the structure function F_2 towards low values of the Bjorken-variable x, much progress has been made in investigating this kinematical regime [3–7]. While the evolution of the structure function with the four-momentum transfer Q^2 is well described by perturbative Quantum Chromo Dynamics (pQCD) for $Q^2 > 1.5$ GeV^2, deviations from pQCD predictions are observed [8] if Q^2 is small, indicating a transition into a regime where non-perturbative effects dominate and the data can only be described by phenomenological models such as those derived from Regge theory [9].

In order to study this non-perturbative regime, the structure function F_2 has been measured at very low values of Q^2, which at HERA are only accessible via special devices mounted close to the outgoing electron[1] beam direction [8] thus facilitating measurements of the scattered electron at very low angles. These low Q^2 data, however, do not cover the transition region at $Q^2 \sim 1$ GeV^2 which up to now has only been examined using "shifted vertex" data taken in 1995 [6].

In this paper the HERA kinematic domain is extended towards low values of Q^2 by making use of DIS events in which a photon is radiated collinear to the incident electron (ISR events). These events, which can be identified by detection of the radiated photon in the small angle photon detector of the luminosity system, effectively have a lower initial electron beam energy and thus, for a given angular acceptance for the scattered electron, allow access to the low-Q^2 regime.

Previous investigations of radiative events at HERA are reported in [4, 10, 11]. The present analysis takes advantage of both improved instrumentation in the backward region in H1 [14], i.e. in the electron direction, and the larger integrated luminosity recorded during the 1997 running period. The presented F_2-measurement covers a kinematic range of $0.35 \leq Q^2 \leq 20$ GeV^2 and $2 \cdot 10^{-5} \leq x \leq 2 \cdot 10^{-2}$. Except for the very low Q^2 regime these data supersede an earlier preliminary analysis based on 1996 data [11].

2 The H1 Detector

The H1 detector [13] consists of a number of subdetectors designed to provide both complementary and redundant measurements of various aspects of high energy electron-proton collisions. Central to this analysis are the backward calorimeter, SpaCal [14], and the H1 luminosity system. The latter consists of two main components, a photon detection system and an electron detector (electron tagger) and is used to determine the luminosity by measuring the cross-section of the Bethe-Heitler reaction $ep \to ep\gamma$. Within the framework of this analysis, it serves to identify ISR events by detecting an energy deposition in the photon detector; the accuracy of the energy measurement provided by the system is $\Delta E_\gamma / E_\gamma = (28 \pm 3)\% / \sqrt{E/\mathrm{GeV}} \oplus 1.0\%$.

[1]During the 1997 data taking period in which the data for this analysis were recorded, HERA provided e^+p collisions. In this paper the incident and scattered lepton are always referred to as "electron".

The scattered electrons in ISR events are detected in the electromagnetic part of the SpaCal calorimeter with an energy resolution of $7\%/\sqrt{E/\mathrm{GeV}} \oplus 1.0\%$. The electron identification is improved by a track requirement based on the information of the backward drift chamber (BDC), which in addition provides a polar angle measurement[2] accurate to 0.5 mrad. The hadronic final state is reconstructed with the LAr calorimeter [15], the tracking detectors and the SpaCal. The total depth of the LAr calorimeter varies between 4 and 8.5 interactions lengths, depending on the polar angle, and provides a hadronic energy resolution of about $50\%/\sqrt{E/\mathrm{GeV}} \oplus 2.0\%$ [16]. In addition, this analysis makes use of the track detectors for vertex reconstruction.

3 Radiative Processes

Radiative processes in ep scattering, as depicted in Figure 1, may be split into three different classes [10, 17] with (i) the bremsstrahlung or Bethe-Heitler process corresponding to small masses of both the virtual electron and the virtual photon, (ii) the QED Compton process with a low virtual photon and a large virtual electron mass and finally (iii) the radiative DIS process at sizeable Q^2 where the photon is collinear either with the incoming (ISR process) or the outgoing (FSR process) electron line.

A set of kinematic invariants taking into account the energy loss from the radiated photon and suitable for describing the process $ep \to e\gamma X$ is given by [12, 18]

$$\hat{Q}^2 = -(p - p' - k)^2 \quad , \quad \hat{x} = \frac{\hat{Q}^2}{2P \cdot (p - p' - k)} \quad , \quad \hat{y} = \frac{P \cdot (p - p' - k)}{P \cdot (p - k)} \quad , \tag{1}$$

where p and P are the four-momenta of the incoming electron and the incoming proton, and p' and k represent the momenta of the scattered electron and the radiated photon, respectively (Fig. 1). Events in which the photon is seen in the photon detector of the luminosity system, i.e. is radiated at very small angles θ_γ with respect to the incident electron beam direction, are dominated by the ISR process. The kinematic quantities defined in (1) are then related to the ep center-of-mass energy squared $s \approx 2Pp$ and the energy fraction $z = (E_0 - E_\gamma)/E_0$ of the electron after the initial photon radiation via

$$\hat{Q}^2 = z\hat{x}\hat{y}s\,. \tag{2}$$

Here, E_0 represents the electron beam energy and E_γ the energy of the radiated photon deposited in the photon detector of the luminosity system.

For the experimental determination of $\hat{x}$, $\hat{y}$ and $\hat{Q}^2$ the kinematics of the scattered electron together with the energy of the radiated photon are used (electron method) with

$$\hat{y}_e = 1 - \frac{E_e}{zE_0}\sin^2\frac{\theta_e}{2} \quad , \qquad \hat{Q}^2_e = 4zE_0E_e\cos^2\frac{\theta_e}{2} \quad , \qquad \hat{x}_e = \hat{Q}^2_e\hat{y}_e/zs \quad , \tag{3}$$

[2]The z axis of the right-handed coordinate system used by H1 is defined to lie along the direction of the incident proton beam and the origin to be at the nominal ep interaction vertex.

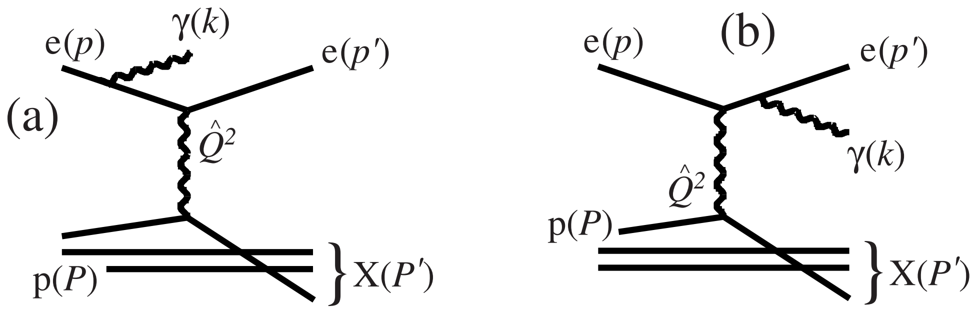

Figure 1: Schematic Feynman diagrams for the radiative process $ep \to e\gamma X$ with (a) initial (ISR) and (b) final state radiation (FSR); p, P represent the four-momenta of the incoming electron and the incoming proton, while p', k and P' are the momenta of the scattered electron, the radiated photon and the hadronic final state X, respectively.

where E_e and θ_e are the energy and scattering angle of the scattered electron. At low values of $\hat{y}$ the resolution of the measurement can be improved by using the hadronic final state kinematics for the determination of $\hat{y}$. This is done with the so-called Σ-method [19], which also reduces the influence of higher order radiative effects. Using $\Sigma_h = \sum_i E_i - p_{i,z}$, where one sums over all hadronic final state objects, and $\Sigma_e = E_e(1 - \cos\theta_e)$ this method yields

$$\hat{y}_\Sigma = \frac{\Sigma_h}{\Sigma_h + \Sigma_e} \quad , \quad \hat{Q}^2_\Sigma = \frac{E_e^2 \sin^2\theta_e}{1 - \hat{y}_\Sigma} \quad , \quad \hat{x}_\Sigma = \hat{Q}^2_\Sigma \hat{y}_\Sigma / zs \quad . \tag{4}$$

Since they are complementary with respect to resolution and their sensitivity to radiative corrections both reconstruction methods presented above were used. The final results are determined using the method which yields the better experimental accuracy in a particular region of phase space.

In terms of the kinematic variables described above, the differential cross section for the ISR process $ep \to e\gamma X$ integrated over the photon emission angle $0 < \theta_\gamma < \Theta_a$ and the energy fraction z reads [12]

$$\begin{aligned} \frac{d^2\sigma}{d\hat{x}d\hat{Q}^2} &= \int_0^{z_{\max}} dz \frac{d^3\sigma}{d\hat{x}d\hat{Q}^2dz} \\ &= \int_0^{z_{\max}} dz \frac{\alpha^3}{\hat{x}\hat{Q}^4} P(z) \left[2(1-\hat{y}) + \frac{\hat{y}^2}{1+R}\right] F_2(\hat{x},\hat{Q}^2)(1+\delta_{\mathrm{RC}}) \end{aligned} \tag{5}$$

where

$$P(z) = \frac{1+z^2}{1-z} \ln\left[\frac{E_0^2\Theta_a^2}{m_e^2}\right] - \frac{2z}{1-z} \quad , \tag{6}$$

$R = F_L/(F_2 - F_L)$ is related to F_2 and the longitudinal structure function F_L, and m_e represents the mass of the electron. In the derivation of equations (5)–(6) all infrared and collinear finite terms have been neglected [12]. Furthermore, terms of order $\mathcal{O}(m_e^2)$ are not taken into account and equation (6) is valid only for angle cutoffs $\Theta_a \gg m_e/E_0$, given by the photon detector acceptance $\Theta_a \approx 0.45$ mrad. Finally, since contributions from Z^0 boson exchange are small for the Q^2 range relevant to this analysis, only pure photon exchange is considered. Radiative corrections of $\mathcal{O}(\alpha^4)$ are represented by the term $1 + \delta_{\rm RC}$.

4 Event Simulation and Higher Order Corrections

Acceptance corrections and background contributions are studied with both the data and Monte Carlo simulations. Radiative and non-radiative DIS events were generated using DJANGO [20]. This program uses HERACLES [21] for simulation of the electroweak interactions and LEPTO [22] to simulate the hadronic final states using the colour dipole model (CDM) as implemented in ARIADNE [23]. The hadronisation is performed with JETSET, which is based on the LUND string model [24,25].

Since HERACLES includes all corrections to deep-inelastic ep scattering up to $\mathcal{O}(\alpha^3)$, the DJANGO program is well suited to generate ISR signal events. Radiative corrections of higher order are, however, not included and were estimated using recent calculations [18,26,27] especially performed for the case of collinear photon radiation off the incident lepton. The calculations were adapted to the specific selection criteria of this analysis and allow the computation of bin-by-bin correction factors for both the electron and Σ reconstruction methods. The resulting correction factors depend strongly on the method used and reach values of 5% (20%) for the Σ–method (electron method).

One of the main difficulties in correctly simulating the ISR signal is the modelling of events in which the measured photon energy is artificially raised by an additional photon from the coincidental overlap of a Bethe-Heitler reaction. For this purpose Bethe-Heitler events were simulated and randomly added to the ISR Monte Carlo according to an overlap probability extracted from the experimental data [28].

The overlap of Bethe-Heitler events with other ep reactions leads to the two main background sources. These are (i) the overlap of bremsstrahlung events with a non-radiative DIS process faking an ISR signature (DISBH) and (ii) γp interactions with an additional Bethe-Heitler overlap (GPBH) where part of the hadronic final state mimics the electron. Photoproduction (GPBH) background is simulated using the PHOJET [29] generator by overlaying real Bethe-Heitler data and the generated sample [28]. For the DISBH background the same method is applied using generated DIS events. For both, an average overlap probability for Bethe-Heitler events with $E_\gamma > 5$ GeV of $4.21 \pm 0.07\%$ was determined.

The detector response of the Monte Carlo events was simulated in detail with a program based on GEANT [30]. After this step the events were subjected to the same reconstruction and analysis chain as the real data.

5 Event Selection

The presented results are derived from data which were recorded during the 1997 data taking period and correspond to an integrated luminosity of 11.1 pb^{-1}. The analysis strategy is based

Item	Cut value
Photon ID	$E_\gamma > 8$ GeV
Electron ID	$E_e > 5$ GeV
	$E_{\text{had}} < 0.5$ GeV
	$R_{\text{clu}} < 3.5$ cm
Background rejection	$\|z\| < 35$ cm, $W > 30$ GeV
	$E_e + E_\gamma < 33$ GeV
	$\|(E_\gamma - E_{\text{miss}})/E_\gamma\| < 0.5$
	$\sum E_i - p_{z,i} < 61$ GeV
	$E_{ET} < 2$ GeV

Table 1: Summary of ISR selection criteria as described in text.

on the detection of a photon in the H1 luminosity system and the requirement of an electron signature in the backward calorimeter, SpaCal. In addition, the selection demands a vertex in the vicinity of the nominal interaction point and places several constraints derived from momentum/energy conservation in order to reduce background due to the overlap of Bethe-Heitler reactions with non-radiative events. The selection criteria are given in Table 1 and summarized in the following:

- **Photon identification:** An energy deposition E_γ above 8 GeV is required inside the photon detector well separated, i.e more than one Moliere radius away, from the edges of the detector.

- **Electron identification:** The scattered electron is assumed to be the cluster of maximum energy E_e in the electromagnetic part of the backward calorimeter. Within a radius of 15 cm of the electromagnetic shower centre there must be no further energy deposition E_{had} of more then 0.5 GeV detected in the hadronic SpaCal. In addition, to guarantee a selection of clean electromagnetic showers, a cut of 3.5 cm is used on the energy weighted cluster radius

$$R_{\text{clu}} = \frac{\sum_i E_i \sqrt{(x_{\text{clu}} - x_i)^2 + (y_{\text{clu}} - y_i)^2}}{E_{\text{clu}}}, \tag{7}$$

  where the sum runs over all cells i of a cluster with energies E_i and coordinates x_i, y_i; x_{clu}, y_{clu} represent the cluster coordinates and E_{clu} is the cluster energy. Finally, an electron candidate must be associated with a track segment in the BDC [3]; thus only clusters within the acceptance of the BDC are subject to the analysis: $156° < \Theta_{\text{BDC}} < 175°$. A minimum energy requirement of $E_e > 5$ GeV is applied.

- **Background rejection:** Only events with a reconstructed vertex with $|z_{\text{vtx}}| < 35$ cm are considered; this substantially reduces contributions from beam-gas and beam-wall interactions. To obtain a reasonably high vertex reconstruction efficiency of more than 90% a cut on the $\gamma^* p$ center-of-mass energy of $W > 30$ GeV is applied to guarantee sufficient hadronic activity in the main detector. This only affects the high-x region and is taken into account in the acceptance calculation. DIS background with overlapping Bethe-Heitler reactions is reduced by requiring $E_e + E_\gamma < 33$ GeV as expected from energy conservation. Since it is required that the scattered electron be seen in the main detector, no energy $E_{\rm ET}$ should be observed in the electron tagger of the luminosity system. This is ensured by requiring $E_{\rm ET} < 2$ GeV. Furthermore, the missing energy in the central detector, $E_{\rm miss}$, must match the energy deposition measured in the photon system such that

$$-0.5 < (E_\gamma - E_{\rm miss})/E_\gamma < 0.5 \ , \qquad (8)$$

where $E_{\rm miss}$ is given by $E_{\rm miss} = E_0 - \frac{1}{2}\sum_i (E_i - p_{z,i})$ with the sum running over all particles seen in the main detector components. Longitudinal momentum conservation implies that $\sum_i E_i - p_{z,i} = 2E_0 \approx 55$ GeV, if summed over all final state particles including the radiated photon. An additional reduction of DISBH and GPBH background is thus achieved by demanding $\sum_i E_i - p_{z,i} < 61$ GeV.

This selection was designed to have a high detection efficiency for radiative DIS events. Within the kinematic range studied the total efficiency is better than 95%. After the final selection $13\,701$ data events remain.

6 Calibration and Background Estimate

Since the selection and kinematic reconstruction rely strongly on the energy measurement in the backward calorimeter, SpaCal, and the photon detector of the luminosity system, the accurate calibration of these detectors is essential for the analysis.

The energy scale of the SpaCal has been carefully determined with QED Compton events using the double angle method for kinematic reconstruction of the energies of the photon and the scattered electron [31]. The remaining uncertainty is 0.5% for energies E_e above 12 GeV and less than 4% for $E_e < 12$ GeV. The results are in good agreement with the calibration used in the most recent F_2 analysis [3]. The photon detector is calibrated using Bethe-Heitler events in which both the photon and the electron were detected in the luminosity system. By fitting the theoretically well known Bethe-Heitler spectrum [32] to the observed photon energy distribution, the absolute energy scale of the photon detector is determined to better than 1% [28]. For the selected event sample, Figure 2 shows several energy and angular distributions for the scattered electron, the tagged photon and the hadronic final state, demonstrating adequate agreement between the data and the Monte Carlo simulation. Concerning the hadronic final state, the calibration is done using the p_t balance between the scattered electron and the hadronic jets, as described in [3, 33, 34]. The remaining differences observed are covered by the experimental systematic errors described below.

The second important issue is the understanding of the different background contributions due to coincidental overlap of DIS and γp reactions with Bethe-Heitler events, as mentioned in section 4. In order to test the modelling of the Bethe-Heitler overlap, and in particular to

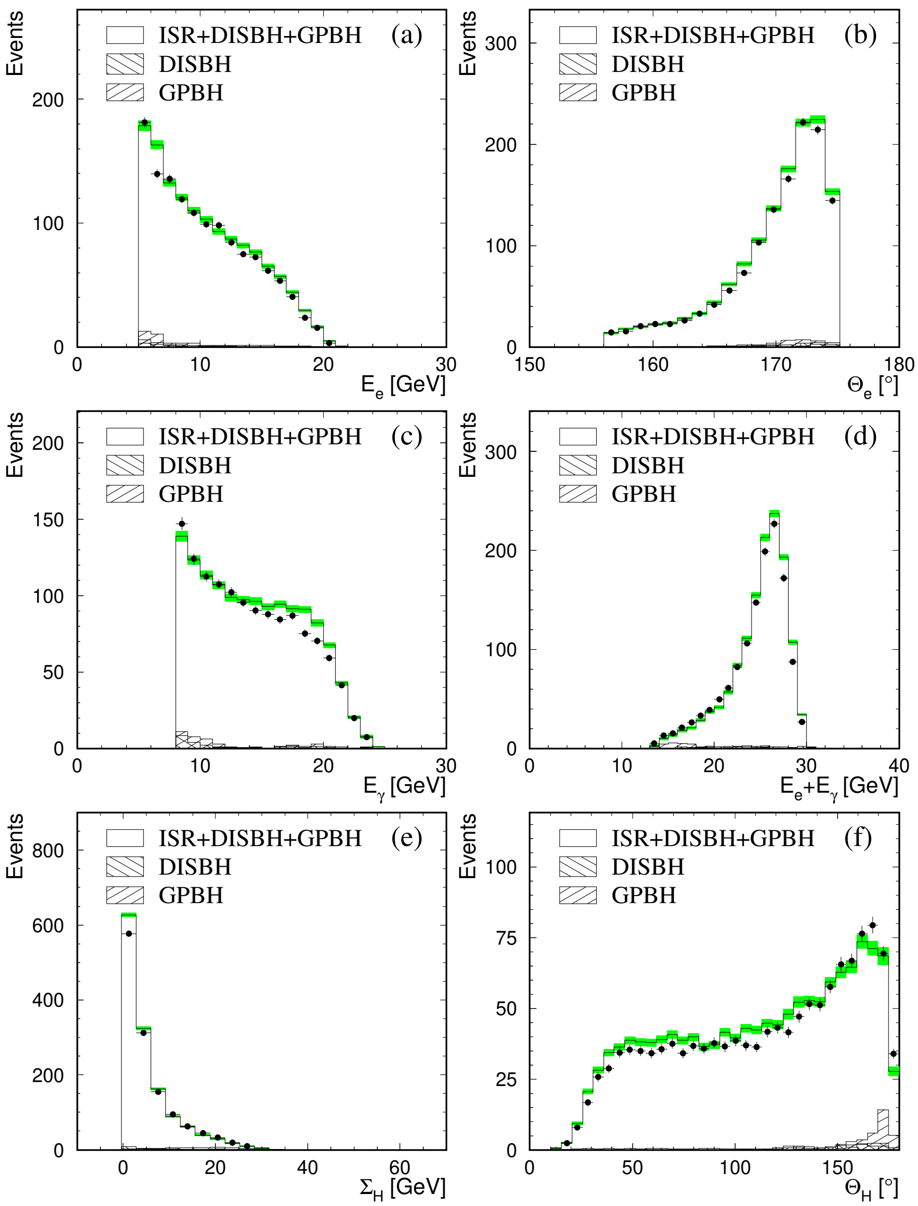

Figure 2: Experimental (points) and Monte Carlo (histogram) distributions of (a) the energy E_e of the scattered electron and (b) the corresponding scattering angle, (c) the energy E_γ of the ISR photon, (d) $E_e + E_\gamma$, (e) the longitudinal momentum balance $\Sigma_H = \sum_i E_i - p_{z,i}$, where the sum runs over all particles of the hadronic final state, and (f) the polar angle Θ_H of the hadronic system. The open histograms show the total Monte Carlo prediction which, in addition to the ISR signal, includes contributions from Bethe-Heitler reactions overlayed with non-radiative DIS processes or photoproduction events. The shaded band indicates the statistical accuracy of the Monte Carlo simulation.

control the normalization of the background Monte Carlo, a clean sample of background events had to be selected. This was possible since 30% of such events can be directly identified by detecting the electron from the Bethe-Heitler reaction. This was done by requiring an energy

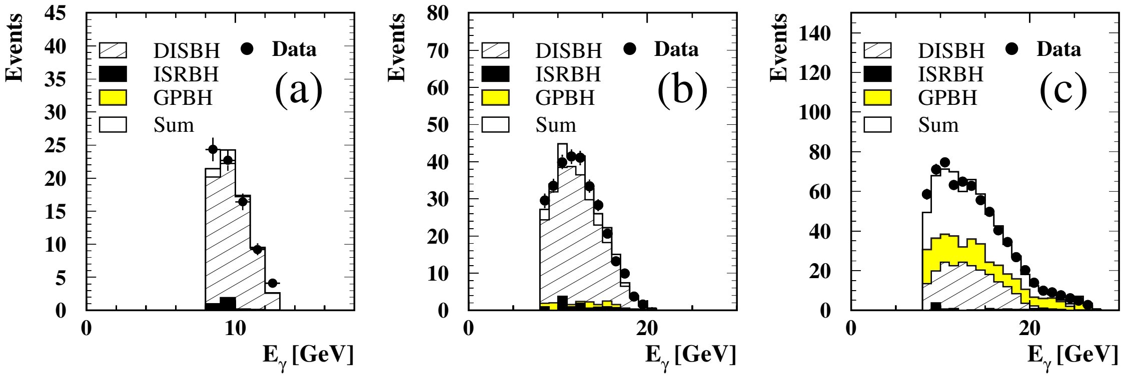

Figure 3: Photon energy distribution for background events with an energy deposition in the electron tagger of the luminosity system for three different energy ranges of the electron candidate seen in the SpaCal: (a) $22 < E_e < 30$ GeV (b) $12 < E_e < 22$ GeV (c) $5 < E_e < 12$ GeV. Data are shown as points, the Monte Carlo prediction for the different background contributions as histograms. As described in section 4, the two main background sources arise from overlap of bremsstrahlung events with the non-radiative DIS process (DISBH) and γp interactions (GPBH). In addition, the ISRBH contribution shown represents signal events with an coincidentally overlapping Bethe-Heitler process in which the electron was seen in the electron tagger. It should be noted that the observed differences between the three E_γ spectra arise from the requirement that the energy sum $E_e + E_\gamma < 33$ GeV, which restricts the photon energy E_γ for higher values of E_e.

deposition E_{ET} above 2 GeV in the electron tagger of the luminosity system. Figure 3 shows the E_γ distribution for these events for three ranges of the energy E_e of the electron candidate seen in the SpaCal; good agreement between data and Monte Carlo is observed. Since the background sample with $22 < E_e < 30$ GeV is dominated by DIS events with Bethe-Heitler overlap, it can be used to check the normalization of the DISBH background. For lower values of E_e there is an additional contribution from GPBH events due to parts of the hadronic final state faking an electron signature. A fit of the E_γ Monte Carlo distributions to the data leads to normalization factors of 0.82 for the DISBH and 1.04 for the GPBH simulation which are applied in Figure 3. The deviation of these normalization factors from one is included in the systematic error of the measurement.

7 Results

In order to extract the structure function F_2 in terms of x and Q^2 the selected data sample is divided into subsamples corresponding to a grid in x and Q^2 as illustrated in Figure 4. The bin sizes are adapted to the resolution in the measured kinematic quantities. They are increased in regions where the number of events is low. Bins are accepted if the purity and stability are greater than 30% with typical values being 50%, where the purity (stability) is defined as the ratio of the number of simulated events originating from and reconstructed in a specific bin to the number of reconstructed (generated) events in the same bin. The proton structure function F_2 was then extracted using a bin-by-bin unfolding method.

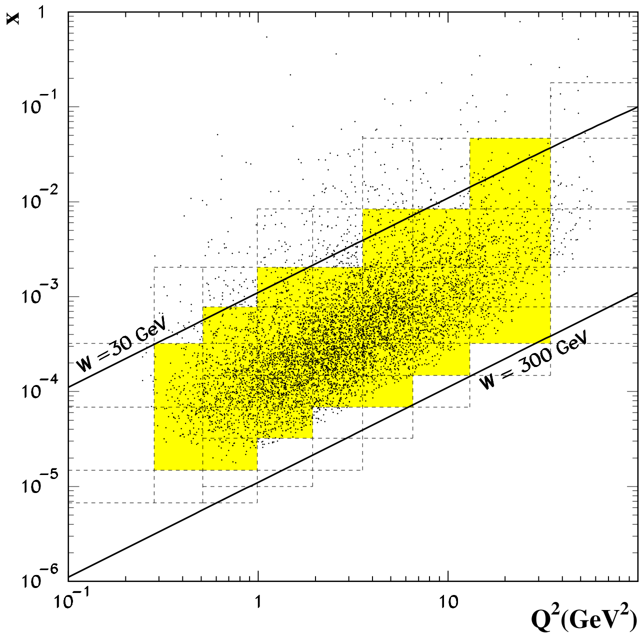

Figure 4: Division of the (x,Q^2)–plane for the measurement of the proton structure function F_2 from radiative DIS events. The figure shows the distribution of the selected ISR events as expected from simulation. The shaded bins are those accepted by the quality criteria described in the text.

With the number of events N ($N_{\rm MC}$) reconstructed in the data (Monte Carlo) and the background contribution, $N_{\rm BG}$, estimated from the DISBH and GPBH Monte Carlo, the numerical value of the structure function at a given point (x,Q^2) is obtained from the ratio $(N - N_{\rm BG})/N_{\rm MC}$ times the corresponding $F_2^{\rm MC}$ value of the parameterization used in the simulation:

$$F_2(x, Q^2) = \frac{N - N_{\rm BG}}{N_{\rm MC}} F_2^{\rm MC}(x, Q^2) \cdot \left(\frac{\mathcal{L}_{\rm MC}}{\mathcal{L}} \right) \frac{1}{1 + \delta_{\rm RC}} \quad . \tag{9}$$

The additional factor $\mathcal{L}_{\rm MC}/\mathcal{L}$ takes account of the different luminosities for data and Monte Carlo, and $\delta_{\rm RC}$ corrects for higher order QED effects not included in the simulation (see section 4). Application of (9) implies a correct modelling of the detector acceptance, selection efficiencies and migrations, which have been carefully checked [28]. The influence of the longitudinal structure function is assumed to be negligible within the kinematic range studied; any impact on the measurement due to this assumption is estimated using the Monte Carlo and included into the systematic error.

Systematic uncertainties have been determined by studying the stability of the results under variation of energy scales and detector resolutions within the accuracies quoted below, variations of selection efficiencies, changes of the background normalization and modification of the theoretical input:

- The electron energy scale is varied by 0.5% for $E_e > 12$ GeV and 2.5% at $E_e = 4$ GeV, where its uncertainty is assumed to decrease linearly in the energy range $4 < E_e < 12$ GeV. This variation leads to an average uncertainty on the F_2 measurement of 3%.
- The uncertainty of 0.5 mrad on the measurement of the polar scattering angle of the electron leads to an uncertainty of about 1% on F_2.

- The uncertainty on the energy scale of the photon detector reaches values up to 1% and leads to an average uncertainty on F_2 of 2.5%.

- The energy resolution of the photon detector is varied within its uncertainty resulting in a 3% systematic error contribution on F_2.

- The accuracy of the hadronic energy scale is influenced by the uncertainties of the energy measurement in the LAr calorimeter ($\pm 4\%$), the energy measurement of the SpaCal ($\pm 5\%$) and the track momenta measured with the tracking detectors ($\pm 2\%$). In total, the hadronic energy scale uncertainty effects F_2 by about 4%.

- The background normalization is known to within 18% and leads to an uncertainty of less than 1% on F_2.

- The modelling of the Bethe-Heitler photon spectrum overlayed with the ISR signal Monte Carlo (see section 4) is done from a minimum photon energy of $E_\gamma^{\min} = 0.15$ GeV, needed to penetrate an active filter placed in front of the photon detector to protect it from synchrotron radiation. The uncertainty on this limit is ± 0.02 GeV and adds about 5% to the systematic error on the final result.

- The vertex reconstruction efficiency is known to about 4 to 5% and leads to a systematic error contribution of 5% to the F_2 measurement.

- Changing F_L in the acceptance calculation from zero to the value resulting from the most recent H1 NLO QCD-fit [3] leads to a variation of the structure function F_2 of 0.8%.

- The estimated uncertainty of the higher order corrections [35] leads to an additional systematic error of 1% on the F_2 measurement.

The total systematic error is determined by summing the individual contributions quoted in quadrature. Finally a 1.5% normalization uncertainty of the luminosity measurement has to be considered, which is not included in the systematic error of the measurement shown in the figures.

The result of the measurement is given in Figure 5 which shows F_2 in bins of x and Q^2 for $2 \cdot 10^{-5} \leq x \leq 2 \cdot 10^{-2}$ and $0.35 \leq Q^2 \leq 20$ GeV^2. The data points are compared to predictions from the ALLM97 parameterization [36], a model based on Regge phenomenology, and the recent H1 QCD-fit [3] to H1 and BCDMS non-radiative F_2 data with $Q^2 > 3.5$ GeV^2. At larger Q^2 the data are well described by the pQCD based H1 parameterization. For Q^2 values below 1 GeV^2 perturbative QCD however fails [3] and only non-perturbative models, e.g. those which incorporate Regge phenomenology, can describe the measurement.

In order to allow comparison with earlier F_2 measurements, Figure 6 shows the Q^2 dependence of the structure function from various analyses at fixed values of the photon-proton centre-of-mass energy W between 25 GeV and 230 GeV. The F_2 data shown in Figure 5 are transformed to the W values given using the ALLM97 parameterization. The results based on

[3] The presented H1 parameterization using $Q^2_{\min} = 3.5$ GeV^2 as starting scale shows deviations from the data at $Q^2 < 3$ GeV^2. It has however been shown that F_2 can successfully be described down to $Q^2 = 1.5$ GeV^2 when $Q^2_{\min}$ is chosen accordingly [3].

the analysis of radiative events span a region which reaches from $Q^2 \geq 1.5$ GeV^2 where pQCD calculations are applicable to the non-perturbative regime, thus probing the transition between DIS and photoproduction within a single data set. The new data are in good agreement with earlier F_2 results both for the low Q^2 domain [8] and the pQCD regime [3]. In the transition region they agree with the earlier H1 result [6]. Data from an earlier preliminary analysis [11] using radiative events from the year 1996 are also shown where they extend this measurement to lower Q^2.

8 Conclusion

Deep-inelastic scattering data with initial state photon radiation are used to extract the proton structure function F_2 for four-momentum transfers $0.35 \leq Q^2 \leq 20\,\text{GeV}^2$ and Bjorken-x values of $2 \cdot 10^{-5} \leq x \leq 2 \cdot 10^{-2}$. The results provide a link between the deep-inelastic scattering (DIS) regime and photoproduction and thus aid the development of an understanding of the transition from regions where pQCD calculations hold into the domain in which non-perturbative effects become large. The measurements are in agreement with previous structure function measurements performed at HERA and with predictions based on a phenomenological approach to the transition region between DIS and photoproduction.

Acknowledgements

We are grateful to the HERA machine group whose outstanding efforts have made and continue to make this experiment possible. We thank the engineers and technicians for their work in constructing and now maintaining the H1 detector, our funding agencies for financial support, the DESY technical staff for continual assistance, and the DESY directorate for the hospitality which they extend to the non DESY members of the collaboration. We also would like to thank H. Anlauf for providing the code to estimate the higher order corrections and for many valuable discussions.

References

[1] I. Abt *et al.* [H1 Collaboration], Nucl. Phys. B **407** (1993) 515.

[2] M. Derrick *et al.* [ZEUS Collaboration], Phys. Lett. B **316** (1993) 412.

[3] C. Adloff *et al.* [H1 Collaboration], hep-ex/0012053.

[4] S. Aid *et al.* [H1 Collaboration], Nucl. Phys. B **470** (1996) 3 [hep-ex/9603004].

[5] M. Derrick *et al.* [ZEUS Collaboration], Z. Phys. C **72** (1996) 399 [hep-ex/9607002].

[6] C. Adloff *et al.* [H1 Collaboration], Nucl. Phys. B **497** (1997) 3 [hep-ex/9703012].

[7] C. Adloff *et al.* [H1 Collaboration], Phys. Lett. B **393** (1997) 452 [hep-ex/9611017].

[8] J. Breitweg *et al.* [ZEUS Collaboration], Phys. Lett. B **487** (2000) 53 [hep-ex/0005018].

[9] P. D. Collins, "An Introduction To Regge Theory And High-Energy Physics", Cambridge 1977, 445p.

[10] T. Ahmed *et al.* [H1 Collaboration], Z. Phys. C **66** (1995) 529.

[11] H1 Collaboration, " Low Q^2 – Intermediate x Structure Function Measurement at HERA", Contributed paper to 29$^{\rm th}$, Conference on High Energy Physics ICHEP 98, Vancouver, Canada, July 1998.

[12] M. W. Krasny, W. Placzek and H. Spiesberger, Hamburg 1991, Proceedings, Physics at HERA, vol. 1, 171-176.

[13] I. Abt *et al.* [H1 Collaboration], Nucl. Instrum. Meth. A **386** (1997) 310 and A **386** (1997) 348.

[14] R. D. Appuhn *et al.* [H1 SPACAL Collaboration], Nucl. Instrum. Meth. A **386** (1997) 397.

[15] B. Andrieu *et al.* [H1 Calorimeter Collaboration], Nucl. Instrum. Meth. A **336** (1993) 460.

[16] B. Andrieu *et al.* [H1 Calorimeter Collaboration], Nucl. Instrum. Meth. A **336** (1993) 499.

[17] A. Courau and P. Kessler, Phys. Rev. D **46** (1992) 117.

[18] H. Anlauf, A. B. Arbuzov, E. A. Kuraev and N. P. Merenkov, Phys. Rev. D **59** (1999) 014003 [hep-ph/9711333].

[19] U. Bassler and G. Bernardi, Nucl. Instrum. Meth. A **361** (1995) 197 [hep-ex/9412004].

[20] G. A. Schuler and H. Spiesberger, Hamburg 1991, Proceedings, Physics at HERA, vol. 3, 1419-1432.

[21] A. Kwiatkowski, H. Spiesberger and H. J. Mohring, Comput. Phys. Commun. **69** (1992) 155.

[22] G. Ingelman, A. Edin and J. Rathsman, Comput. Phys. Commun. **101** (1997) 108 [hep-ph/9605286].

[23] L. Lönnblad, Comput. Phys. Commun. **71** (1992) 15.

[24] H. Bengtsson and T. Sjöstrand, Comput. Phys. Commun. **46** (1987) 43.

[25] T. Sjöstrand and M. Bengtsson, Comput. Phys. Commun. **43** (1987) 367.

[26] H. Anlauf, A. B. Arbuzov, E. A. Kuraev and N. P. Merenkov, JHEP **9810** (1998) 013 [hep-ph/9805384].

[27] H. Anlauf, Eur. Phys. J. C **9** (1999) 69 [hep-ph/9901258].

[28] C. Issever, Dissertation, Universität Dortmund, Dortmund (2000).

[29] R. Engel and J. Ranft, Phys. Rev. D **54** (1996) 4244 [hep-ph/9509373].

[30] R. Brun *et al.*, CERN-DD/EE-84-1.

[31] V. Lendermann, Dissertation, Universität Dortmund, in preparation.

[32] G. L. Kotkin, S. I. Polityko, A. Schiller and V. G. Serbo, Z. Phys. C **39** (1988) 61.

[33] A. A. Glazov, Dissertation, Humboldt Universität, Berlin (1998).

[34] R. Wallny, Dissertation, ETH Zürich, in preparation.

[35] H. Anlauf, privat communication.

[36] H. Abramowicz and A. Levy, DESY-97-251, hep-ph/9712415.

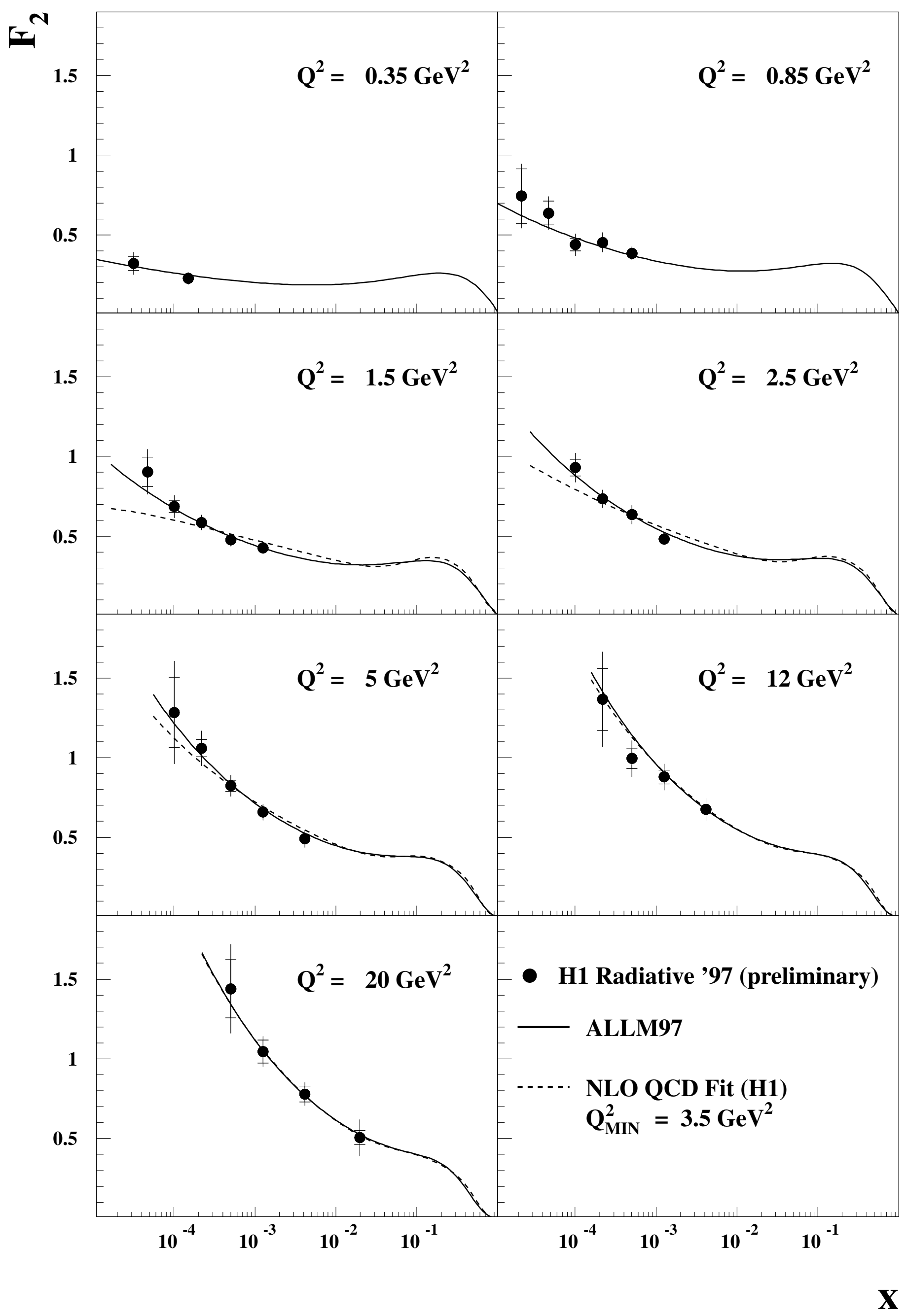

Figure 5: The structure function F_2 as determined from ISR events as a function of x for fixed values of Q^2. The inner error bars represent the statistical and the outer error bars the total uncertainty of the measurement. The data are compared to the ALLM97 (solid curve) parameterization and the most recent H1 NLO QCD fit to non-radiative F_2 data (dashed curve) starting at $Q^2_{\rm MIN} = 3.5$ GeV^2 [3].

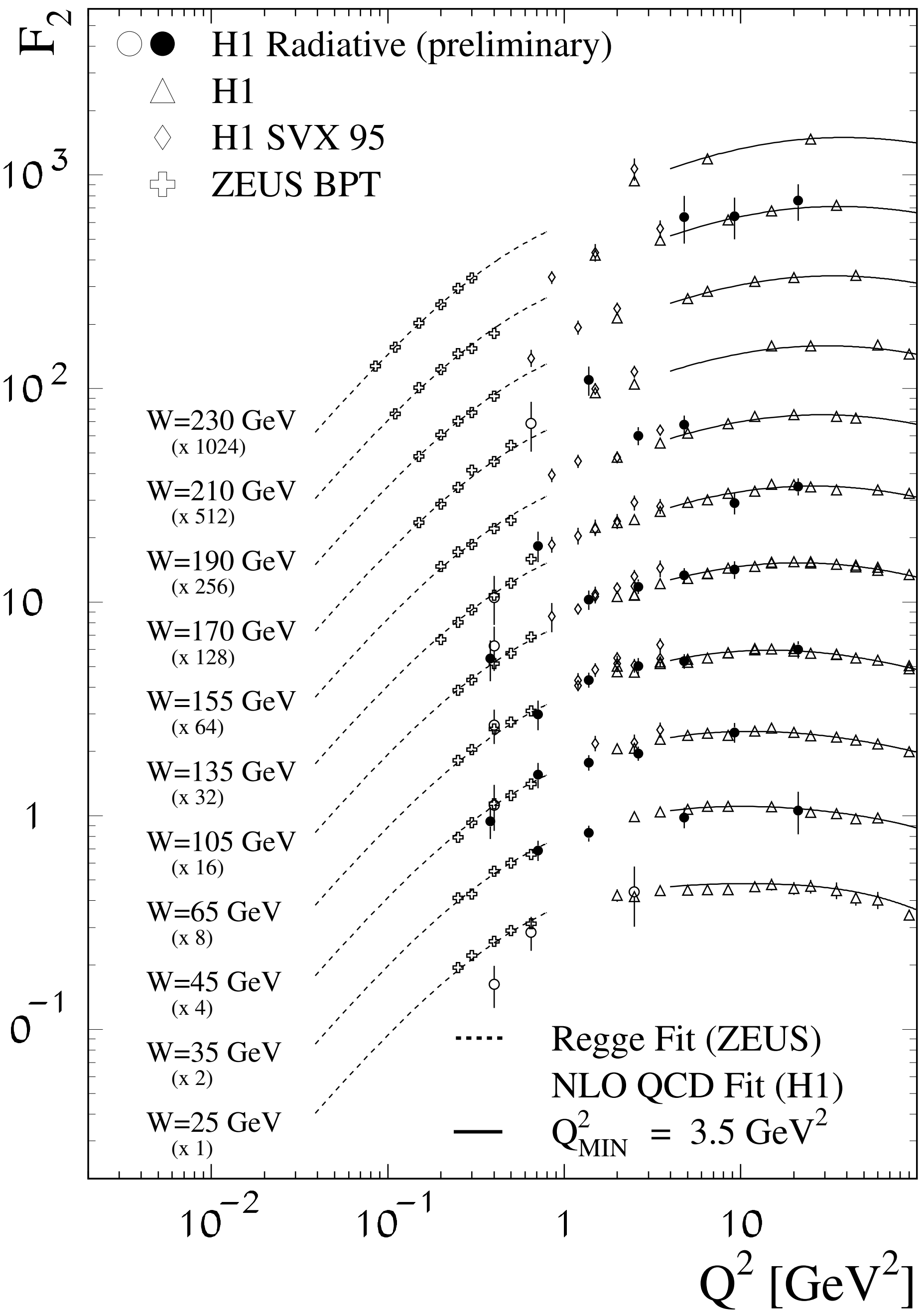

Figure 6: The structure function F_2 as a function of Q^2 for fixed values of W. ISR measurements (closed circles: this analysis; open circles: H1 radiative 96 [11]) are shown together with the 96/97 nonradiative F_2 results of H1 [3] (triangles), the F_2 shifted vertex 95 data [6] (diamonds) and the low Q^2 results from ZEUS [8] (open crosses). The measurements are compared with the ZEUS Regge fit (dashed curve) and with the H1 NLO QCD fit to the non-radiative F_2 data (solid curve) starting at $Q^2_{\rm MIN} = 3.5$ GeV^2 [3].